Development of an eddy current distance sensor for high temperature environments

Michael Schmid
Master of Applied Research in Engineering Sciences
Deggendorf Institute of Technology
94469 Deggendorf, Germany
Email: michael.schmid@stud.th-deg.de

Werner Frammelsberger
Faculty of Mechanical Engineering and Mechatronics
Deggendorf Institute of Technology
94469 Deggendorf, Germany
Email: werner.frammelsberger@th-deg.de

***Abstract*—The desire for high temperature (HT) capabilities of electronic devices continues to grow steadily. Rugged designs are demanded, especially in sensor technology applications with integrated circuits trending. Sensors need to perform accurately and reliably under extreme conditions like temperatures up to 200 °C. In this work, an eddy current sensor for distance measurements in HT-environments is developed and tested. Individual components and circuit segments are specifically designed or selected to prevent premature device failure and thermal drift.**

***Index Terms*—High Temperature, Eddy Current Sensor, Distance Measurement, Packaging and Interconnection Technology**

I. Introduction

Sensors are an integral part of control loops and enable regulation of fabrication processes and product monitoring. They need to perform precisely within their specifications and reliably over their expected lifetime. Major challenges, which increase with operation temperature, are device degradation, measurement imprecision, long term drifting and hysteresis. In order to meet the growing industrial HT demand, this work deals with the development of an eddy current sensor for the 200 °C benchmark. The sensor system is supposed to be implemented in a single carrier and includes the sensor and the associate electric circuits. This work reports the conceptual design of the system, the research for suitable components, appropriate assembly and connection technology as well as the manufacturing of a test system and associated tests. For the sake of briefness, this article concentrates on the overview and the key features of the system rather than to present conceptual details of the development process. As the literature survey alone includes more than a hundred sources, details are presented in the project reports and will be summarized in a final thesis. In addition, specific simulation models are presented that predict the sensor behavior at 200 °C. Measurement results of the test system are compared with the simulations in order to create a miniaturised prototype via iterational improvement.

II. Sensory principal

The measuring principle of the sensor is based on the theory of eddy currents [1]. This is a current induced in an electrical conductor within a magnetic field. The principle is used by an integrated coil, which is fed with a high-frequency alternating current (AC) signal. This coil forms an electromagnetic field whose field lines emerge from the sensor plane. If an electrically conductive object approaches the sensor plane, the field lines penetrate it and induce eddy currents. Those currents create an electromagnetic field in the object, which counteracts the field of the coil and change the coil impedance. Amplitude and phase of the sensor signal hinge on the coil impedance, which is part of a resonant circuit in the sensor. The closer the object, the greater the influence. A possible total penetration of the measuring target by the field lines as well as omnidirectional pre-damping of the LC resonant circuit (RC) are considered. Fig.1 shows the distance information acquisition by phase position evaluation. A rectangular reference signal

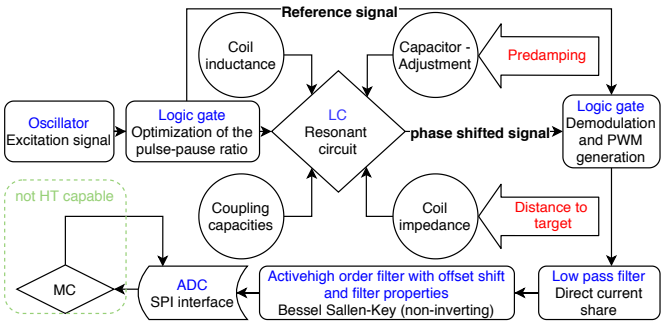

Fig. 1. Block diagram of the sensor principle

is compared with a phase-shifted sinusoidal signal by means of a demodulator. From the resulting puls width modulation (PWM) carrier frequency, a direct current (DC) voltage is extracted, amplified and filtered. The prototype covers a surface of 462,6 mm^2. The lower measuring range (MBA) is 50 µm and the upper (MBE) 230 µm at an average resolution of 10 nm. The lifetime at 200 °C is estimated to be 1000 hours.

III. Literature And Market Research

The following subsections are a brief summary. (cf. [2])

A. Carrier And Sensor Design

The main component of every eddy current sensor is the coil. Here, the coil is implemented in a multi-layer structure within the carrier for the electronic circuit. Due to limited space, three layered meander coils are series-connected to achieve the measuring range needed. The layers have to

be interconnected with conductive material filled microvias to counteract barrel failures. Only a single-sided component placement is possible. Roughly 35 % of the surface is usable for component placement. Therefore, small surface mounted devices (SMD) or dies are used. Except for capacitor adjustment (CA), it is not planned to rework the sensors after manufacturing. To reduce voiding defects and softening, the solder employed needs to be easily spreadable and highly wetting with an eutectic point well above 200 °C. Fatigue failure of SMD solder joints will most likely not be an issue, as mechanical vibration and stress occurs predominantly perpendicular to the devices. The solder needs to match the coefficient of thermal expansion (CTE) of the components.

B. Carrier Platform Technology

Tab.I lists properties of ceramic platforms. Advantages are the thermal-mechanical behavior such as CTE, thermal conductivity, aging under the influence of temperature changes, heat capacity and high glass transition temperature (Tg) [3]. Ceramics do not decompose at HT in contrast to polymers and

TABLE I
PROPERTIES OF CERAMIC CARRIER MATERIALS AT 25 °C [2]

Material	**Al_2O_3**	**Green Tape 951**	**Si_3N_4**	
Tg	2050	900	1400	[°C]
CTE	8	5,8	2,5	[Ppm/°K]
Length strength	375	320	900	[N/mm]
Cross strength	375	320	535	[N/mm]
Dielectric const.	9,4	7,8	9,2	at 1 MHz
Surface resist.	10^{14}	10^{12}	10^{14}	[Ω]
Cost factor	8	7	10	to FR4

epoxides. Their chemical bonding does not suffer from heat and UV-radiation, nor do ceramics soften or absorb moisture to any significant extent [4]. Low Temperature Cofired Ceramics (LTCC) are relative low cost compared to Al_2O_3 or Si_3N_4. One example of application is the DuPont Green Tape 951 as stacked layers. Every layer is cut into the preferred shape. Conductor paths between the layers usually consist of Au or Ag thick film pastes and are silk-screen printed onto the unfired carriers. With respect to costs and availability other common organic PCBs were also considered (Tab.II). In essence, or-

TABLE II
PROPERTIES OF CONVENTIONAL CARRIER MATERIALS AT 25 °C [2]

Material	**CEM3**	**FR4**	**Polyimide**	**Teflon**	
Tg	125	135-210	250	270	[°C]
CTE	190	170	40	100	[Ppm/°K]
Length stre.	355	600	110	600	[N/mm]
Cross stre.	300	490	100	490	[N/mm]
Diele. const.	4,5	4,2-5,4	3,8	2,7	at 1 MHz
Surf. resist.	10^6	10^{11}	10^{11}	10^{11}	[Ω]
Cost factor	2	1	5	3,5	to FR4

ganic materials can only withstand HT to a limited extent and have poorer dielectric properties. Furthermore LTCCs possess a comparatively small CTE which is required to minimize mechanical stress. Due to its outstanding properties regarding the current application, LTCC was chosen for the prototype.

C. Component Substrate

The properties of active electronic components (ECs) can change considerably at HT because of increasing charge carrier densities in the substrate [5]. Since associated effects are particularly critical in conventional silicon technology, devices with silicon on insulator (SoI) technology are frequently used for HT and are adopted here. In SoI technology, diffusion effects and leakage currents are reduced by a complete spatial isolation of the individual electronic device by oxide layers within the substrate. This is to counteract the increasing influence of these effects at HT. Passive ECs, like resistors, are appropriate for use at HT in thin or thick film Al_2O_3 technology. The correct function of the electronic circuit depends on the properties of all HT components exposed to temperatures up to 200 °C. Particular importance is attributed to permissible deviations from the nominal values and the subsequent deration. Extensive research was undertaken to provide a complete overview of available hardware for the use at HT [2].

D. Die Attach

Die attachment is the mounting of a die on a lead frame substrate or carrier. Within common die attach technologies, a distinction (Tab.III) can be made between epoxy adhesives, soft- and eutectic soldering as well as silver-glass metal or alternative resins [6]. Considering the precarious situation

TABLE III
AVAILABLE HIGH TEMPERATURE SOLUTIONS FOR DIE ATTACH [2]

Material	**T** $[°C]$	**K** $[W/cmK]$	**CTE** $[ppm/K]$	**G** $[GPa]$
Au80Sn20	250	0,58	16	68
P-1011	350	0,0129	37	-
H20E-HC	200	0,0996	53	-
QMI-3555R	300	0,8	16	11,5
FO3, FO13	300	0,6	25	-
Tape 3M	350	-	-	0,1
Ag nano	500	2,4	19	9

around leaded solder and the associated environmental impact as well as lack of available equivalent alternatives, glue is used to attach the die. An electrically conductive adhesive (ECA) enriched with Ag nano-particles offers the best overall Tg, CTE, heat conduction and strength. The bonding surface on the LTCC is coated with Ag to avoid intermetallic phases (IMCs).

E. Die Bonding

There are several ways to electrically connect a chip. Wirebonding was chosen for the specific application. Usually Au-wire bonding is used in industrial production. However, since the passivation of most dies consist of AlCu, IMCs would form over a few hours at HT [7]. This is known as purple plague (AuAl, Au_2Al, Au_8Al_{23}, Au_4Al, $AuAl_2$). High Resolution Transmission Electron Microscopy has shown that even at 175 °C the IMCs are growing rapidly and after about an hour there is a continuous layer [8]. The Al-pad is entirely consumed within 10 hours. Subsequently, the vertical IMCs shift, but the transverse growth continues and exceeds the bond after 25 hours. Au-bonding is therefore not an option

for HT applications. Al, Cu, Pd and Ag were considered as alternative materials (Tab.IV). With regard to conductivity and

TABLE IV
PROPERTIES OF AVAILABLE WIRE METALS

Properties	Au	Al	Cu	Pd	Ag	Unit
Tg	1063	660	1083	1552	962	[°C]
Thermal cond.	195	230	395	75	430	[w/mK]
CTE	14	23	16	10	18,9	[ppm/K]
El. resistance	2,20	2,49	1,72	10,75	1,59	[$\mu\Omega$/cm]
Rel. conductivity	78	69	100	16	108	[%] to Cu

minimization of IMC formation, Cu is best suited. With an inert gas atmosphere an Au similar Free Air Ball bond is possible with Cu wires. Pd is only suitable to a limited extent due to high cost and low conductivity. Al has advantages like high thermal conductivity and reduced material costs. Detriments of Al are a large CTE and formation of an oxide layer. The bonds are less ductile and susceptible to fractures

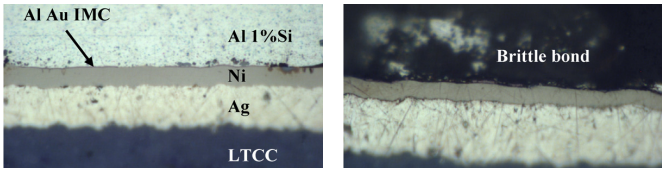

Fig. 2. Sectional view of LTCC with Al-wire bond [9]

when compared to Au, while only Wedge-Wedge bonding is possible. IMCs (Fig.2) still form to a limited extent and will harm lifetime expectations but remain in an acceptable range. In summary, Al wire bonding technology was chosen due to cost efficiency and accessible production machines.

F. Die Protection

The modalities of housing the die depend on the environment in which the sensor is used. There are several recommendations for potting or protective measures [10]. If there is no harmful atmosphere, a casting can be avoided. To protect the wirebonds, a housing made out of polyimid is sufficient. If protection against chemicals or vibration is required, this encapsulation can be filled with potting compounds. Like Dam&Fill this allows the use of materials with different viscosity, Tg and CTE. The prototype is only capped to avoid potential aging effects of the filling altering any measurements.

IV. RESONANT CIRCUIT CALCULATION

The calculation and simulation of the resonant circuit is an important part of the sensor development process, predominately in order to evaluate the influence of the operation temperature. To make an estimation of the temperature dependent RC performance, the sensor coils embedded in the LTCC were soldered with a hotplate onto a four-wire measurement setup (Fig.3) and connected to a compensated measuring bridge. A temperature ramp within the climatic chamber resulted in a change in series inductance (L_S) and resistance (R_S). The characteristics of the sensor were used to calculate coupling

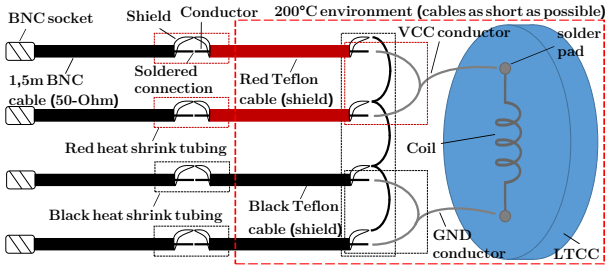

Fig. 3. Schematic representation of the four-wire measurement

(C_S), decoupling and the RC (Fig.4) to obtain a PWM, mainly affected by the CA. Referring to Fig.4 a transfer function (Eq.1) was established. Real and imaginary part (Eq.2,3) were

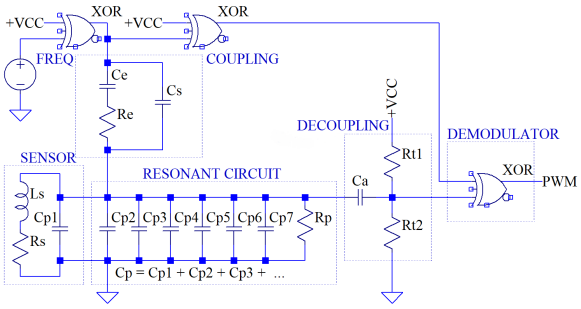

Fig. 4. Functional diagram of the phase evaluation

complex conjugated. The magnitude and phase are calculated using Eq.4. According to Fig.5 a CA with maximum and homogeneous sensitivity for MBA and MBE has been chosen.

$$H = \frac{Z_1}{Z_1 + Z_2} = \frac{\frac{1}{j\omega C_P + \frac{1}{j\omega L_S + R_S}}}{\frac{1}{j\omega C_P + \frac{1}{j\omega L_S + R_S}} + \frac{1}{j\omega C_S}} \quad (1)$$

$$Re = \frac{\omega^4 C_S^2 L_S^2 + \omega^4 C_S L_S^2 C_P - \omega^2 C_S L_S + \omega^2 C_S^2 R_S^2 + \omega^2 C_P^2 R_S^2 + 2\omega^4 C_S L_S^2 C_P + 2\omega^2 C_S R_S^2 C_P + \omega^2 C_S^2 R_S^2 + \omega^2 C_S R_S^2 C_P}{+\omega^4 C_S^2 L_S^2 - 2\omega^2 C_S L_S + \omega^4 C_P^2 L_S^2 - 2\omega^2 C_P L_S} \quad (2)$$

$$Im = \frac{\omega C_S R_S \cdot 1}{1 + \omega^2 C_S^2 R_S^2 + \omega^2 C_P^2 R_S^2 + 2\omega^4 C_S L_S^2 C_P + 2\omega^2 C_S R_S^2 C_P + \omega^4 C_S^2 L_S^2 - 2\omega^2 C_S L_S + \omega^4 C_P^2 L_S^2 - 2\omega^2 C_P L_S} \quad (3)$$

$$\text{Magnitude} = \sqrt{Re^2 + Im^2} \qquad \text{Phase} = \arctan\frac{Re}{Im} \quad (4)$$

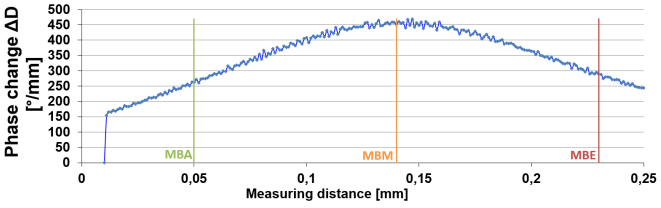

Fig. 5. Phase change over temperature with ideal CA

V. Test System

A HT test system was developed and manufactured.

A. Circuit Concepts

The test system includes, in addition to the shown RC excitation, a setup with D-FlipFlops for a more constant duty cycle. For the amplifier, filter and offset-shift, a non-inverting Bessel Sallen-Key is used. With this topology, overshoots are avoided at the expense of increased gate delay. The test system provides an amplifier of the second, third and fourth order. Optionally with floating offset to achieve the maximum voltage control. The circuit temperature can be read out via a PT1000, using an amplified voltage divider, wheatstone differential amplifier, phase demodulation and four-wire measurement. The system also possesses various supply and reference elements. On request, sensor and temperature signal are switched to an ADC via a control pin. The 16 bit ADC is controlled by a µC.

B. High Temperature Simulation Models

Furthermore, detailed models were designed in LTspice to predict the behavior of the sensor system under HT influence [11]. Therefore, either replacement models of components were created, or manufacturer models were customized. The operational amplifier can thus map a temperature dependent offset voltage and input bias current. Additionally, specific adapted components like all digital gates, sources and other individual components such as oscillators were specifically adapted to model their HT performance. The simulation models support an AC analysis in open and closed-loop operation and not only allow for a temperature-specific evaluation of the DC behavior of the system, but also support an AC analysis in open and closed-loop operation.

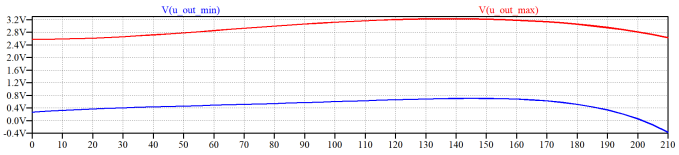

Fig. 6. DC-magnitude at MBA (blue) and MBE (red) over Temerature [°C]

VI. Conclusion

The eddy current sensor and the test system developed was tested by a furnace run between 0 °C and 180 °C. The measurement results were in good agreement with simulations as well as calculations and meet the expectations. This was specifically the case for the control unit of the sensor measuring range. Concerning the sensitivity at MBA and MBE, the test system showed only a small deviation to the calculated values, most likely caused by coupling capacities and pre-attenuation. The filter topologies behaved very similar to the simulations and proved to be stable for different pre-defined measuring ranges and over the complete temperature range tested. The amplification showed minor deviations to expected values, resulting in a decreased measurement resolution of the following ADC. However, this was solely caused by the cautious amplifier design in combination with extreme value simulations in order to guarantee operation over the whole temperature range. The most promising concepts for a miniaturized sensor system were adapted on a LTCC. According to the results of sec.III, the miniaturized prototype (Fig.7) was created by use of the selected assembly and connection technologies. Even though the promising results show the validity of the concept the miniaturized prototype must be tested in detail.

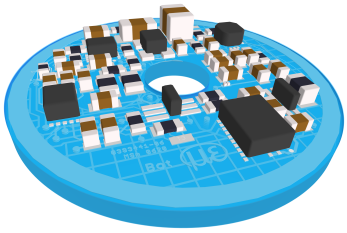

Fig. 7. Render representation of the prototype

Acknowledgment

I want to thank my colleagues at Micro Epsilon GmbH & Co. KG for the pleasant working environment and always offering a helping hand. Also my project leader Dr. Junge for hinting me in the right direction when necessary. Special thanks towards my supervisor Prof. Frammelsberger, without whom I would have never participated in the MAPR program.

References

[1] E. Schrüfer, "Elektrische Messtechnik - Messung elektrischer und nichtelektrischer Größen", 11. Edition, Hanser Verlag, Wien, Okt. 2014.

[2] M. Schmid, "Literature research regarding electronic design and packaging technology for hybrid high temperature applications", TH Deggendorf, Deggendorf, Projectreport 1, p. 85, Jan. 2020.

[3] T. Bartnitzek, T. Thelemann, S. Apel, und K.-H. Suphan, "Advantages and limitations of ceramic packaging technologies in harsh applications", International Symposium on Microelectronics, Bd. 2016, Nr. 1, S. 000581–000585, Okt. 2016, doi: 10.4071/isom-2016-THP23.

[4] S. Brosius und A. F. Jacob, "LTCC material properties after high temperature treatment", in 2013 European Microwave Conference, Okt. 2013, S. 436–439, doi: 10.23919/EuMC.2013.6686685.

[5] R. Wittmann, "Miniaturization Problems in CMOS Technology: Investigation of Doping Profiles and Reliability", TU Wien, Wien, 2007.

[6] M. Arifin, N. Wivanius, und N. F. Prebianto, "Epoxy Adhesive as Die Attach Material in Semiconductor Packaging: A Review", in 2018 International Conference on Applied Engineering (ICAE), Okt. 2018, S. 1–5, doi: 10.1109/INCAE.2018.8579410.

[7] H. Xu u. a., "New mechanisms of void growth in Au–Al wire bonds: Volumetric shrinkage and intermetallic oxidation", Scripta Materialia, Bd. 65, Nr. 7, S. 642–645, Okt. 2011, doi: 10.1016/j.scriptamat.2011.06.050.

[8] H. Xu u. a., "Intermetallic phase transformations in Au–Al wire bonds", Intermetallics, Bd. 19, Nr. 12, S. 1808–1816, Dez. 2011, doi: 10.1016/j.intermet.2011.07.003.

[9] R. Johannessen, F. Oldervoll, und F. Strisland, "High temperature reliability of aluminium wire-bonds to thin film, thick film and low temperature co-fired ceramic (LTCC) substrate metallization", Microelectronics Reliability, Bd. 48, Nr. 10, S. 1711–1719, Okt. 2008, doi: 10.1016/j.microrel.2008.06.008.

[10] Y. Yao, G.-Q. Lu, D. Boroyevich, und K. D. T. Ngo, "Survey of High-Temperature Polymeric Encapsulants for Power Electronics Packaging", IEEE Transactions on Components, Packaging and Manufacturing Technology, Bd. 5, Nr. 2, S. 168–181, Feb. 2015, doi: 10.1109/TCPMT.2014.2337300.

[11] M. Schmid, "Simulation of an high temperature eddy current sensor", TH Deggendorf, Deggendorf, Projectreport 2, p. 135, Jul. 2020.